Journal of Electroanalytical Chemistry 819 (2018) 502–510

Contents lists available at ScienceDirect

Journal of Electroanalytical Chemistry

journal homepage: www.elsevier.com/locate/jelechem

Probing the $Fe^{n+}/Fe^{(n-1)+}$ redox potential of Fe phthalocyanines and Fe porphyrins as a reactivity descriptor in the electrochemical oxidation of cysteamine

Nataly Silva[a,*], Sebastián Calderón[a], Maritza A. Páez[a], María P. Oyarzún[a], Marc T.M. Koper[b,*], José H. Zagal[a,*]

[a] Laboratorio de Electrocatálisis, Departamento de Química de los Materiales, Facultad de Química y Biología, Universidad de Santiago de Chile, Casilla 40, Correo 33, Santiago 9170022, Chile
[b] Leiden Institute of Chemistry, Leiden University, PO Box 9502, 2300 RA Leiden, The Netherlands

ARTICLE INFO

It is a great honor for us to dedicate this manuscript to a very outstanding electrochemist, the late Professor Roger Parsons FRS.

Keywords:
Cysteamine electrooxidation
Fe phthalocyanines
Tuning the redox potential
Activity volcano correlations

ABSTRACT

The $M^{n+}/M^{(n-1)+}$ redox potential of MN4 macrocyclic molecular catalysts is a very good reactivity descriptor for several electrochemical reactions. One important feature about this reactivity descriptor is that it can be determined experimentally under the same conditions of the kinetic measurements in contrast to other descriptors like intermediate binding energies that are estimated from DFT calculations. However a linear correlation between both descriptors seems to exist. Plots of activity as $(\log j)_E$ at constant E versus the $M^{n+}/M^{(n-1)+}$ redox potential gives volcano correlations. Another important aspect about this parameter is that it is possible to tune the $M^{n+}/M^{(n-1)+}$ redox potential of the MN4 catalyst by manipulating the structure of the macrocyclic complex and tailoring the electron-withdrawing power of the ligands to obtain the maximum activity. In this work we have probed the redox potential as a reactivity descriptor for the oxidation of cysteamine studying a series of substituted Fe phthalocyanines and Fe porphyrins adsorbed on glassy carbon and pyrolytic graphite in alkaline media. As expected the catalytic activity of these FeN4 species varies strongly with the Fe (II)/(I) redox potential of the different Fe phthalocyanines and a plot of activity as $(\log j)_E$ versus $E°$Fe(II/I) gives a volcano-shaped correlation so a formal potential value exists for which the highest activity can be achieved demonstrating that the formal potential of the complexes seems to be an universal reactivity descriptor for electrochemical reactions.

1. Introduction

Reactivity descriptors and activity volcano correlations are very important issues in the fundamentals of electrocatalysis as they establish reactivity guidelines for developing and creating more active electrocatalytic surfaces for specific electrochemical reactions, especially as these sort of reactions are involved in fuel cells, air batteries and several industrial electrochemical processes. Professor Roger Parsons made very important contributions in this field [1,2] and it is with pleasure that we dedicate this manuscript to his memory, especially as we will discuss some reactivity descriptors for MN_4 macrocyclic metal complexes that belong to the class of molecular catalysts. Macrocyclic MN_4 complexes such as metallophthalocyanines (MPcs) and metalloporphyrins (MPs) possess extended electronic π-system capable of undergoing fast reversible electron-transfer processes centered on the metal and on the ligand [3,4] due to the very low reorganizational energies involved. They are very versatile materials that catalyze a series of electrochemical reactions when confined on the surface of carbon and graphitic materials and their activity has been discussed in many publications [4–20]. Electrocatalytic reactions are inner-sphere electron transfer processes as they involve the formation of a covalent bond between the reactant/intermediate and some atom or active site on the electrode surface and this facilitates electron transfer due to the overlap of frontier electronic molecular orbitals. This is not the case for outer-sphere reaction and their kinetics are independent of the nature of the electrode [3]. For the case of metal electrodes (an alloys) a classical an important reactivity descriptor is the binding energy of the reacting molecule or some reaction intermediate to the metal site [1,2,21–27]. For the particular case of MN_4 metal complexes this is also valid for the reduction of O_2 [28] but little work has been done along these lines for other reactions [4]. However an interesting reactivity descriptor of MN_4 macrocyclic complexes is the

* Corresponding author.
E-mail address: jose.zagal@usach.cl (J.H. Zagal).

https://doi.org/10.1016/j.jelechem.2017.12.068
Received 5 August 2017; Received in revised form 26 December 2017; Accepted 29 December 2017
Available online 03 January 2018
1572-6657/

$M^{n+}/M^{(n-1)+}$ redox potential. In general it involves the M(III)/(II) and M(II)/(I) redox couples depending on the reaction. For some reactions the onset potential appears very close to the $M^{n+}/M^{(n-1)+}$ redox potential so this parameter acts as a switch since only one of the oxidation states of the metal is catalytically active. When the potential of the electrode containing these catalysts is scanned so the overpotential increases, as soon as traces of the active species start to form as a result of the applied potential, the reaction commences [29]. The interesting thing about this reactivity descriptor is that it can be measured under the same conditions of the experiment, i.e. with the metal complexes confined on the surface of a suitable rather inert electrode like graphite or glassy carbon, in contact with the electrolyte that is used for the kinetic measurements. In general it is believed that the active site for many reactions is the M(II) state. In contrast, the M(III) state is inactive so for reduction reactions like O_2 reduction the M(III)/(II) redox potential determines the onset for the reaction as the reaction occurs on incipient M(II) species that start to form during the negative potential scan. The opposite is true for oxidation reactions where the M(II)/(I) redox potential determines the activity. In this work we want to probe the Fe(II)/(I) redox potential as an activity descriptor for the oxidation of cysteamine. Cysteamine is a biologically relevant molecule [30] and active electrodes for the electrooxidation of cysteamine can potentially serve as electrochemical sensors for detecting this biologically important molecule [31–38]. Cysteamine is an aminothiol which has the formula $HSCH_2CH_2NH_2$. It is the simplest aminothiol and also it is a drug used to treat cystinosis as it depletes L-cystine that can build up in cells of people that suffer from this disease.

2. Experimental

2.1. Materials

The iron (II) 1.2.3.4.8.9.10.11.15.16.17.18.22.23.24.25-hexadecacloro-29*H*.31*H*-phthalocyanine (16(Cl)FePc), iron (II) 2.9.16.23-tetra(amino) phthalocyanine (FeTAPc), iron (II) 2.9.16.23-tetra(nitro) phthalocyanine (FeTNPc), iron (III) 5.10.15.20-(tetra-4-methoxyphenyl) porphyrin chloride (FeTMeOP), iron (III) 5.10.15.20-(tetra-4-pyridyl) porphyrin chloride (FeTpyP) were obtained from PorphyChem, and iron phthalocyanine (FePc) was obtained from Sigma Aldrich. All the metal complexes were used as provided.

Multi-walled carbon nanotubes (MWCNTs) were acquired from Dropsens (diameter 10 nm. and length of 1–2 μm). MWCNTs were purified in 37% HCl solution for 5 days and then refluxed for 5 h. followed by thoroughly washing with water. Acetone, *N.N* dimethylformamide (DMF) (analytical grade), NaOH and cysteamine (≥ 98.0%) were provided by Sigma-Aldrich. Electrolyte solutions were prepared with MilliQ water (Millipore. Inc.).

2.2. Preparation of hybrid materials between MWCNTs and iron complex

The hybrid materials between FePc or FeP complex and MWNTC were obtained using methodologies reported previously [39]. MWCNTs were dispersed in phthalocyanines (1 mg mL^{-1}) by sonication for 30 min. The suspensions were left to rest for 24 h. at room temperature and were then filtered and washed with the corresponding solvent and ethanol to remove any excess of the complex. The solid was dried in an oven at 40 °C for 24 h. Finally MWCNTs + MPc suspensions in DMF (1 mg mL^{-1}) were prepared.

2.3. Electrochemical measurements

The working electrode (Pine Instrument) was a glassy carbon electrode (GC) with a geometrical area of 0.196 cm^2. We also used a pyrolytic graphite electrode (OPG) to characterize the $Fe^{n+}/Fe^{(n-1)+}$ redox processes of the adsorbed complexes. The cyclic voltammograms obtained with OPG were similar to those obtained when using glassy carbon but the cyclic voltammetry profiles were better defined on OPG. A platinum spiral wire and Ag/AgCl, 3 M electrode were used as the auxiliary and reference electrodes respectively. Electrochemical measurements were performed on a Bas CV-100W Voltammetric Analyzer using a conventional three-compartment glass cell. The electrolyte was a N_2 saturated 0.1 M NaOH solution at a temperature of 25 °C.

Cyclic voltammetry (CV) were used to verify the correct functionalization of the electrodes. Slow linear sweep voltammetry (0.05 V s^{-1}) was used to determine the polarization curves for the oxidation of cysteamine on the different electrodes studied. Polarization curves were obtained in N_2 saturated solutions. Scan rate 0.005 V s^{-1}.

2.4. Preparation of modified electrodes

Before each experiment the surface of the GC electrode was mechanically polished with alumina suspension followed by ultrasonic treatment in purified water for 2 min and dried with nitrogen flow. GC was modified with different metal phthalocyanines or metal porphyrins placing a drop (10 μL) of the $1 \cdot 10^{-4}$ M solutions of the complexes or 1 mg mL^{-1} of the hybrid materials. All the complex solutions were prepared using DMF. For all modifications the electrodes were thoroughly washed with DMF to eliminate any excess of the complex.

3. Results and discussion

Fig. 1 illustrates the structures of Fe phthalocyanines and Fe porphyrin bearing different substituents on the ligand used in present work. The purpose of using different substituents on the ligand is to affect or tune in different ways the electron density on the Fe center, depending on whether these groups are electron-donating or electron-withdrawing compared to the −H group in the un-substituted Fe phthalocyanine.

All these complexes were tested with the macrocyclics pre-adsorbed on ordinary pyrolytic graphite electrodes as the response on OPG gives better defined redox peaks than in GC. The response of the clean OPG is rather flat, except at around − 0.15 V where a very weak signal can be observed and can be attributed to redox processes involving quinonic groups or other functionalities that exists at defects of the graphite surface [40]. When the electrode is modified with different FeN4 complexes two distinct signals are observed in the potential range from − 1.6 to 0.2 V: signal **1** is attributed to the Fe(II)/(I) reversible couple whereas signal **2** is assigned to the Fe(III)/(II) reversible transition. It is important to point out that recently it has been suggested that signal **1** could be also attributed to a reversible charge transfer process occurring on the ligand without the involvement of the Fe center as Fe(II)Pc/$Fe(II)Pc^{-1}$ [41] so this possibility cannot be discarded. As expected, as the electron-withdrawing power of the groups located on the ligand increases the redox processes shift in the positive direction. Electron-withdrawing groups on the ligand lower the energy of the electronic orbitals of the complex including the frontier orbital from where the electron is removed. So more energy (more positive redox potential) is required to remove that electron for the *d*-character frontier orbital of FeN_4.

Fig. 3 shows a series cyclic voltammograms similar to those of illustrated in Fig. 2 but with the Fe complexes pre-adsorbed on MWCNTs and the MWCNT deposited on OPG. The response is essentially similar and the redox processes are not affected much by the nature of the supporting substrate whether its OPG or MWCNTs. It is important to comment that the MWCNTs were modified with the Fe complexes separately before incorporating the MWCNT to the OPG substrate. The MWCNTs contribute to increase the amount of FeN4s on the electrode by a factor of ca. 10 compared to the amount of complexes adsorbed on the smooth OPG surface. As a consequence the currents observed for the MWCNT/FeN_4 hybrid electrodes are much larger and nearly 10 times more intense than for the OPG/FeN_4 electrodes.

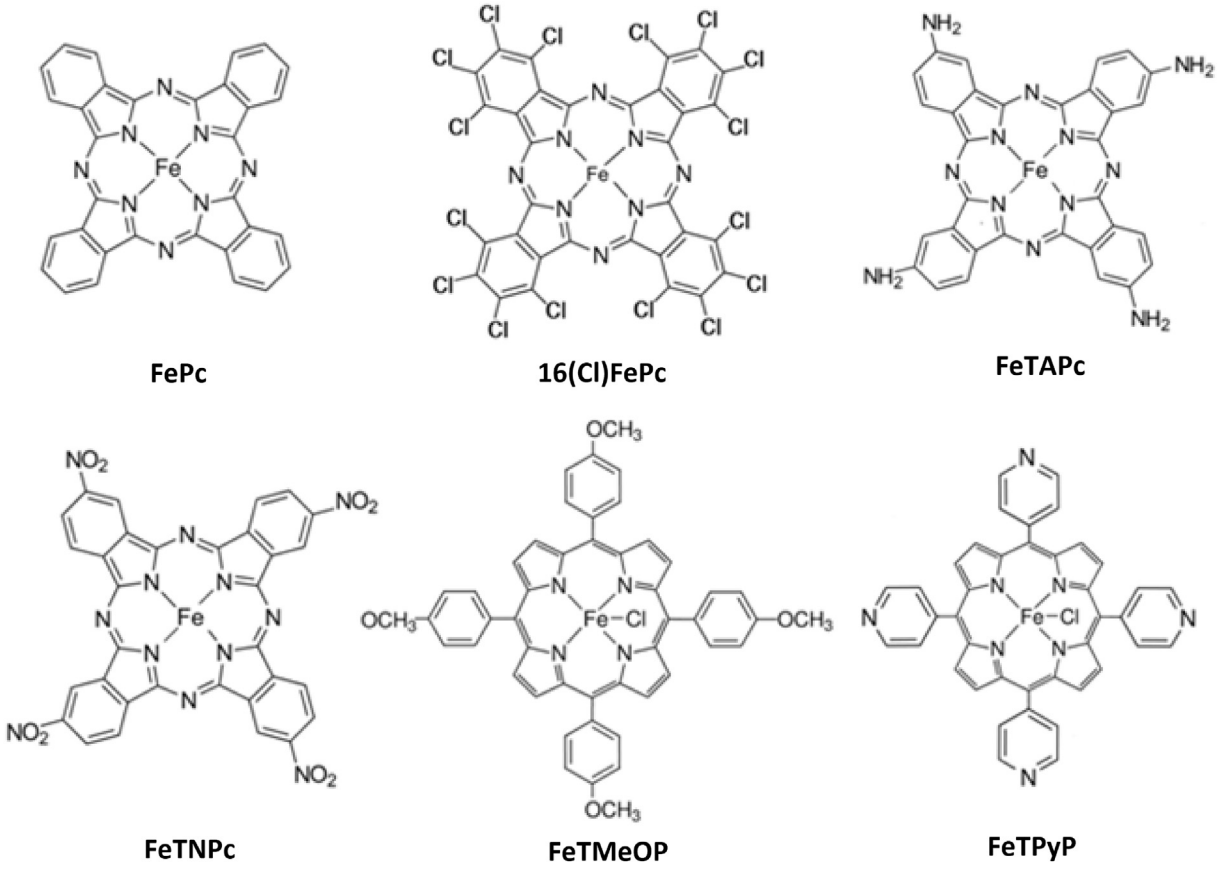

Fig. 1. Structures of the studied iron complexes (phthalocyanines and porphyrins) bearing different substituents.

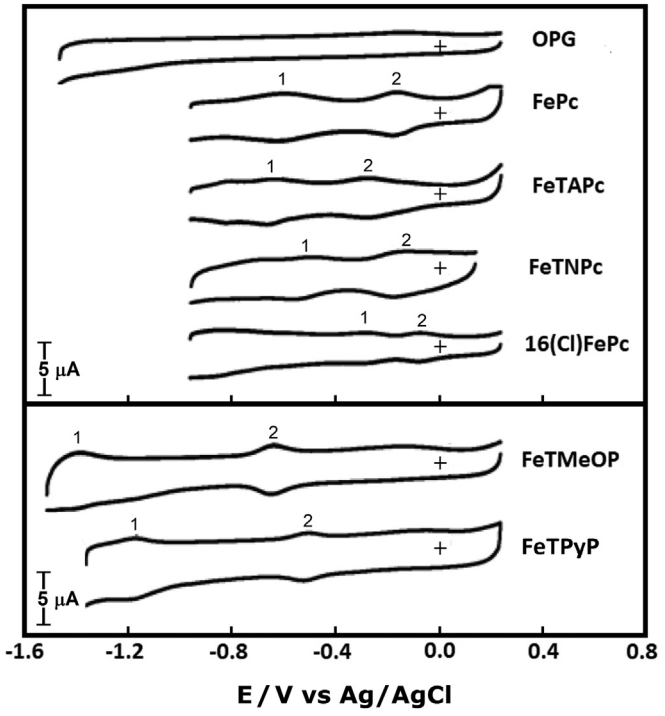

Fig. 2. Cyclic voltammograms of a OPG electrode modified with FePs and FePcs and recorded in deaerated, N_2 saturated 0.1 M NaOH aqueous solution. Adapted from Fig. 6 [39]. Scan rate 0.1 V s^{-1}.

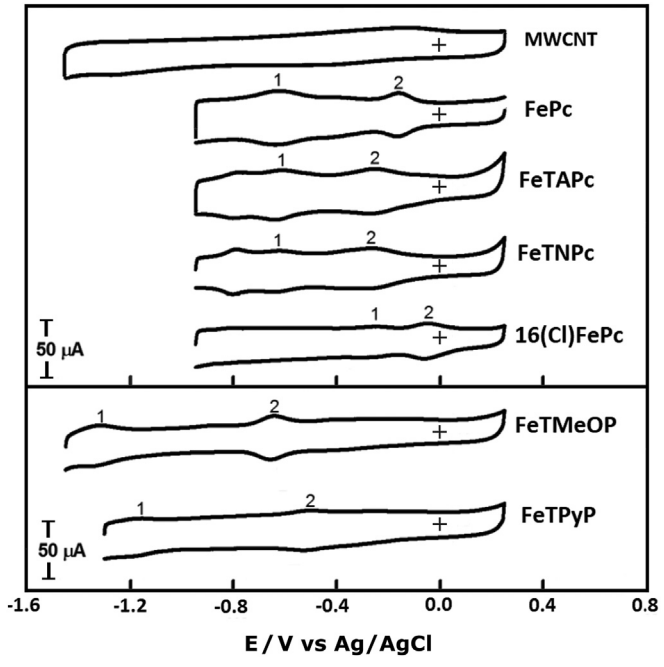

Fig. 3. Cyclic voltammograms of a GC electrode coated with MWCNT modified with FePs and FePcs and recorded in deaerated, N_2 saturated 0.1 M NaOH aqueous solution. Adapted from Fig. 6 [39]. Scan rate 0.1 V s^{-1}.

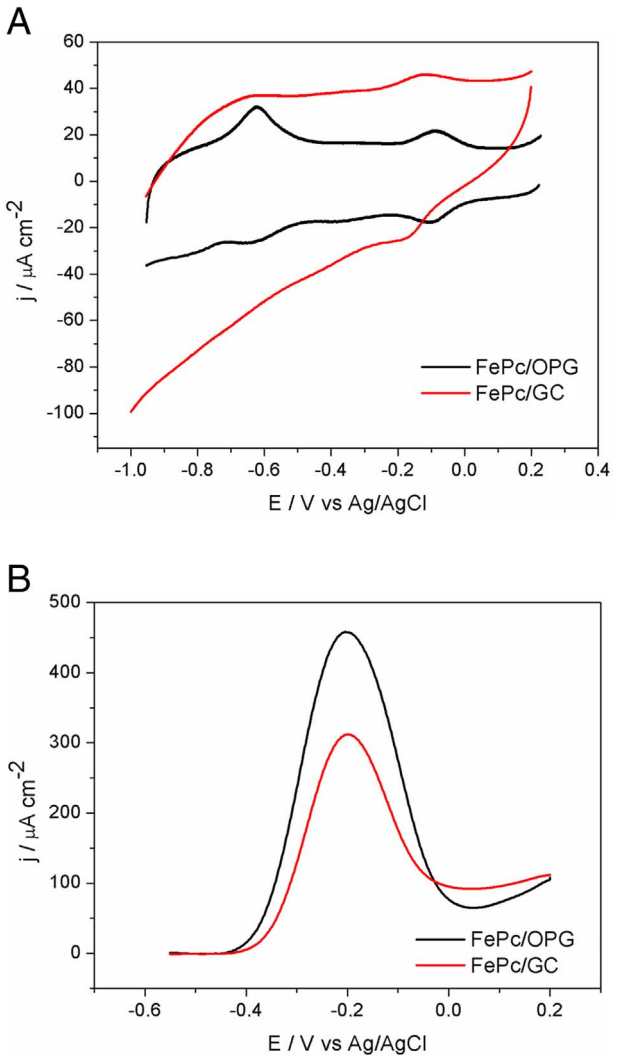

Fig. 4. Cyclic voltammograms of FePc adsorbed on GC and OPG electrodes (NaOH 0.1 M, N_2 saturated solution; scan rate = 0.1 V s^{-1}) (a). Polarization curves for the oxidation of 5 mM cysteamine on GC and OPG electrodes modified with FePc (0.1 M NaOH, N_2 saturated; scan rate 0.005 V s^{-1}, rotation rate = 1000 rpm) (b).

Fig. 4a compares the potentiodynamic response of two kinds of electrodes modified with FePc: OPG and glassy carbon (GC). We wanted to compare these two types of electrodes as especially scientists working in electroanalysis more commonly use GC than OPG in the literature. The figure on the left shows the responses of both FePc/OPG and FePc/GC. The CV curve of FePc/OPG is more flat than that of FePc/GC and less capacitive. Both redox processes are well defined on OPG. In contrast GC shows higher capacitive currents and less defined redox processes. This difference can be attributed to the less homogeneous and more open structure of GC compared to OPG [42]. Fig. 4b shows the polarization curves for these two electrodes when 5 mm of cysteamine is added to the electrolyte. The polarization curves on both electrodes are very similar but the intensity is different. The maximum current for FePc/OPG is 460 μA whereas for FePc/GC is only 300 μA and the lower response could attributed to the lower total concentration of FePc compared to OPG as evidenced by the weaker redox signals of FePc/GC shown on the cyclic voltammograms in Fig. 4a. The polarization curve was obtained on a rotating disk electrode and the absence of a typical diffusional plateau can be attributed to the oxidation center from Fe (II) to Fe (III)OH^- at E = − 0.1 V which is not far from − 0.2 V. the current maximum in the polarization curve. The (III) state has no catalytic activity because the active sited is blocked by adsorbed OH^-. This has been observed for other electrochemical reactions

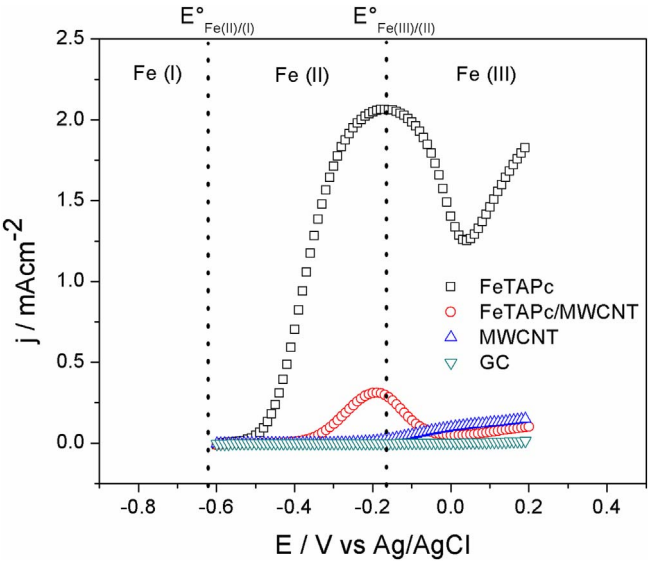

Fig. 5. Polarization curves of the oxidation of 5 mM cysteamine in 0.1 M NaOH for GC electrode modified with FeTAPc and MWCNT/FeTAPc. The formal potentials of FeTAPc are indicated by dotted lines. Scan rate = 0.005 V s^{-1}.

catalyzed by FeN4 complexes like the oxidation of L-cysteine and glutathione [39] where the thrill group RSH is oxidized to RSSR and cysteamine is not an exception. This type of behavior is also illustrated in Fig. 5 where the polarization curves for the oxidation of cysteamine were obtained on a smooth GC electrode modified with FeTAPc and on GC modified with MWCNTs modified with FeTAPc. The maximum current for the FeTAPc/MWCNT/GC electrode is about 10 times larger than that obtained with the FeTAPc/GC electrode so again a factor of ca. 10 is observed for the currents obtained when using MWCNTs and can be attributed to a 10 times larger concentration FeTAPc per geometric area compared to the smooth FeTAPc/GC electrode, assuming that the reaction is first order in $[Fe(II)N4]_{ad}$.

Fig. 6 illustrate the polarization curves obtained on a GC electrode modified with the iron macrocycles (a) and the corresponding hybrids (b). It is observed that every curve has a maximum current that quickly drops at more positive potentials and this was discussed before for Fig. 5 so for all catalysts, inhibition is observed at potential where Fe (III)OH starts to form on the electrode surface and this is also observed for the electrodes having carbon nanotubes. In the latter case the drop in the currents is less pronounced when MWCNTs are present.

Fig. 7 shows Tafel plots obtained with data taken from the zone of kinetic control. It is observed in Fig. 7 that these slopes are similar to one another for most of the FePcs while values for FePs are almost double and could attributed to a change in mechanism that will be discussed further on (see Table 1). A similar analysis can be done from Fig. 4b where the data was obtained with the complexes adsorbed on carbon nanotubes. The slopes values of ~0.060 V/decade are found for FePcs while FePs show values of > 0.120 V/decade. The Fe porphyrins show the lowest activity of all complexes studied.

As discussed in the introduction the Fe(II)/(I) redox potential is a good reactivity descriptor and the catalytic activities can be compared versus this parameter. Fig. 8 shows a plot of $(\log j)_E$ at a constant potential (0.3 V) versus the formal potential of the Fe(II)/(I) redox couple of each catalyst. The correlations in Fig. 8 have the typical volcano shape of plots of the activity of metal electrodes versus the binding energy of intermediates to the active site [2,23,24]. In previous work [28] when comparing the activity for O_2 reduction of a great variety of MN_4 complexes we have found that the M(III)/(II) formal of the catalysts correlates with the M−O_2 binding energy in a linear fashion. It is possible and this will be checked in future work that the binding energies of cysteamine to different MN4 complexes also correlate in a

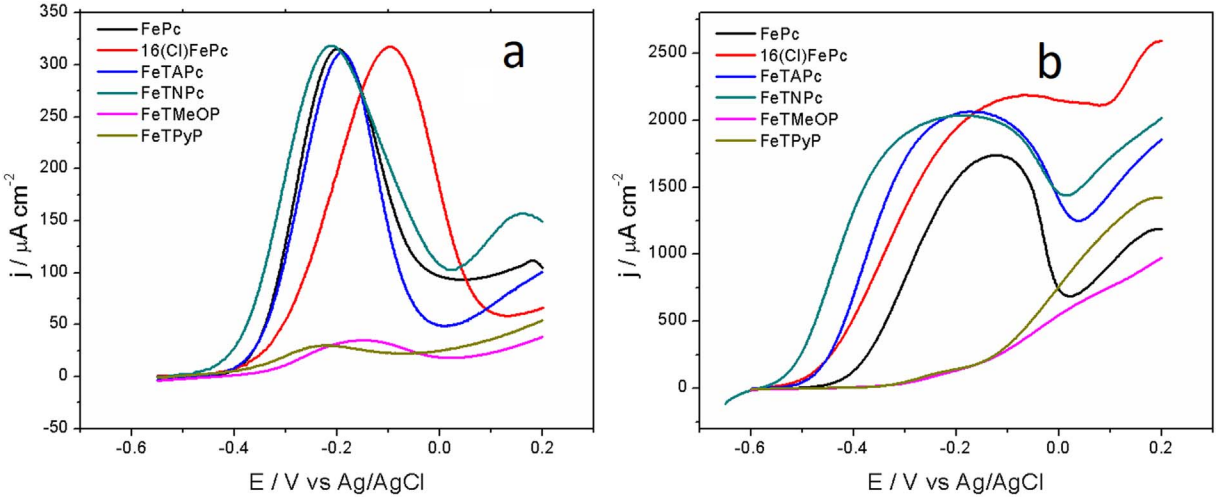

Fig. 6. Polarization curves obtained from oxidation of cysteamine 5 mM in = 0.1 M NaOH on electrodes of (a) GC modified with FePcs and FePs; and (b) GC modified with MWCNT/FePcs and MWCNT/FePs. N_2-saturated solution; scan rate: 0.005 V s^{-1}. Rotation rate: 1000 rpm.

linear fashion with the formal potential of the catalyst.

There are two zones clearly defined: a rising region which corresponds to the FePs complexes and a falling one where FePcs are located. In this trend, hypothetically complexes with formal potentials near the summit of the volcano should present higher activity for the cysteamine oxidation reaction so once more, this illustrates the concept we have proposed before that it is possible to "tune" the formal potential of a MN4 catalyst in order to obtain the maximum activity. However, in our case there are two catalysts on one side of the volcano correlation, specifically FeTMeOP and FeTPyP that have Fe(III)/(II) formal potentials that are far too negative compared to the potential chosen for comparing activities, i.e. − 0.3 V so at this potential not all surface confined FeN4 catalyst are in the Fe(II) active form. The surface coverage of Fe(II) as a function of the Fe(III)/(III) and Fe(II)/(I) formal potentials is given by the Nernst equation for adsorbed species, assuming ideal behavior.

$$\theta(\mathrm{Fe(II)}) = \frac{\exp(F(E - E^0_{II/I})/RT)}{[1 + \exp(F(E - E^0_{II/I})/RT)]} \frac{1}{[1 + c_{OH^-}\exp(F(E - E^0_{III/II})/RT)]} \quad (1)$$

θ(Fe(II)) at $E = -0.3$ V can be calculated for FeTMeOP and FeTPyP adsorbed on OPG and on GC/MWCNT. When the complexes are confined on GC for FeTMeOP $\theta(\mathrm{Fe(II)}) = 10^{-6.748}$ and for FeTPyP θ(Fe(II)) = $10^{-4.5}$. When the complexes are confined on GC/MWCNTs for FeTMeOP $\theta(\mathrm{Fe(II)}) = 10^{-7.01}$ and for FeTPyP $\theta(\mathrm{Fe(II)}) = 10^{-5.03}$. These very low values of θ(Fe(II)) indicate that the low activities of Fe porphyrins can be attributed to a very low surface concentration of Fe (II) active sites and explains the volcano correlation. These two complexes appear on the "strong adsorption" side of the volcano correlation and their low activity cannot be attributed to the classical explanation of low coverage of Fe[II] free sites due to thermodynamically favourable adsorption of RS· radicals on the Fe(II) sites but simply to a shift in the $RS_{(aq)}^- + [Fe(II)N_4]_{ad} \Leftrightarrow [Fe(II)N_4RS]_{ad} + e$ equilibrium to the reactants side due to a very low concentration of $[Fe(II)N_4]_{ad}$ species. An interesting correlation is obtained if the currents for these two porphyrins are divided by θ[FeII] at that particular potential. The volcano correlations in Fig. 8 become straight lines and the interesting thing is that the slopes for GC/FeN4 and GC/MWCNT/FeN4 electrodes are − 0.090 V and − 0.129 V/decade respectively which are close to the theoretical value of $-RT/\beta' F$ (− 0.118 V/decade) assuming that the Brönsted coefficient β = 0.5. The low activity of FeTMeOP and FeTPyP is then attributed to the fact that most of the catalyst at the potential of comparison is in the wrong oxidation state of Fe(III)OH and its low activities are due to the strongly bound OH^{-1} to the Fe(III) center that prevents cysteamine molecules to interact with the active

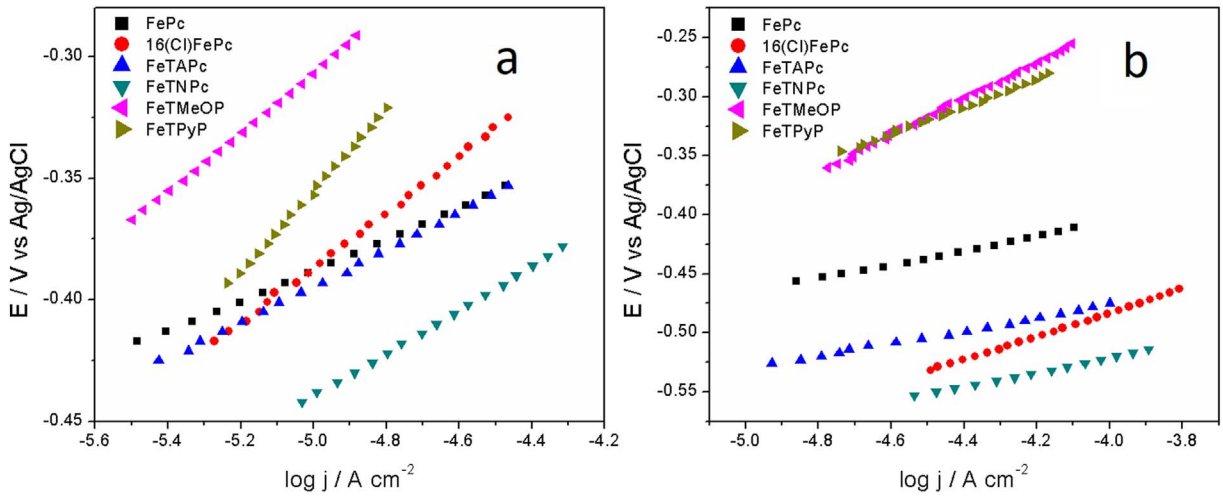

Fig. 7. Tafel slopes obtained from polarization curves for oxidation of cysteamine 5 mM in NaOH 0.1 M on GC electrodes modified with (a) FePcs and FePs; (b) MWCNT + FePcs and MWCNT + FePs (b).

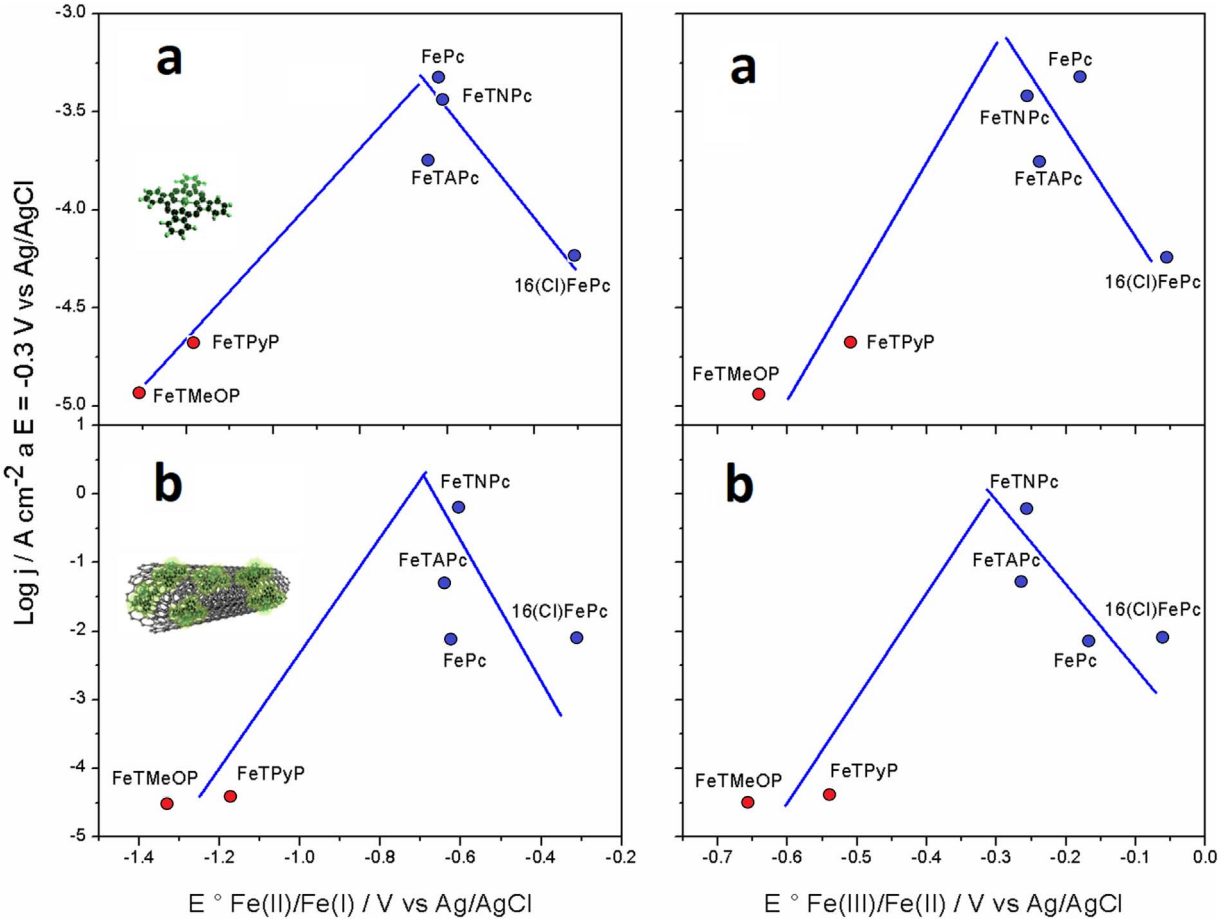

Fig. 8. Log*j* (E = − 0.3 V) versus the *E°'*Fe(II)/(I) and *E°'*Fe(III)/(II) formal potential of the catalyst for the electro-oxidation of cysteamine using GC electrodes modified with (a) FePcs y FePs; (b) with MWCNT/FePcs and MWCNT/FePs.

site.

We may develop a simple model for the catalyst dependence of the rate of cysteamine oxidation following Parson's original ideas [1] assuming the following mechanism, in which RHS represents cysteamine:

$$RSH_{(aq)} + OH^-_{(aq)} \Leftrightarrow RS^-_{(aq)} + H_2O \quad (2)$$

$$RS^-_{(aq)} + [Fe(II)N_4]_{ads} \Leftrightarrow [Fe(II)N_4 - RS]_{ads} + e^- \quad (3)$$

$$[Fe(II)N_4 - RS]_{ads} \rightarrow [Fe(II)N_4]_{ads} + RS^{\cdot} \quad (4)$$

$$2\,RS^{\cdot} \rightarrow RSSR \quad (5)$$

where we assume that the final product of cysteamine electrooxidation is the cysteamine disulfide. In this mechanism, we assume that the Fe (II) state of the adsorbed phthalocyanine or porphyrin is the catalytically active state (Fig. 9).

If the pH is constant and higher than the pK_a of RSH, $c(RHS^-_{(aq)}) = c$,

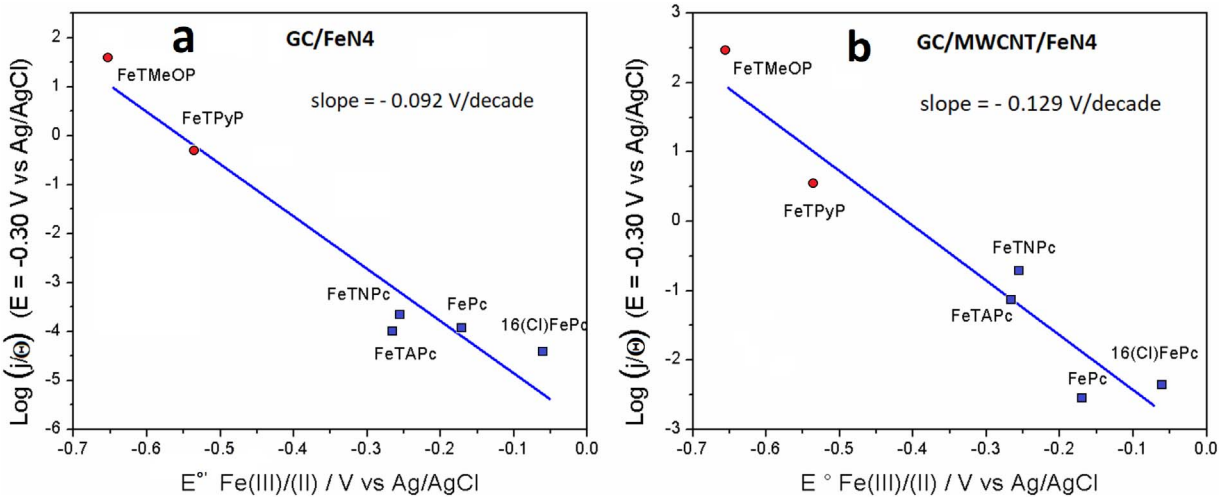

Fig. 9. Log (*j*/*θ*) (E = − 0.3 V) versus *E°'*Fe(III)/(II) formal potential of the catalyst for the electro-oxidation of cysteamine using GC electrodes modified with (a) FePcs y FePs; (b) with MWCNT/FePcs and MWCNT/FePs.

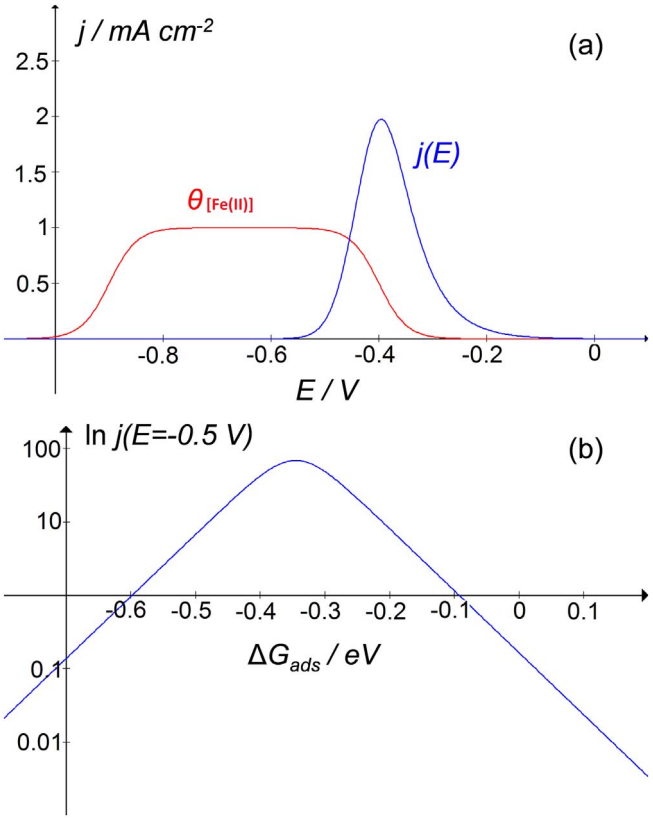

Fig. 10. Simulated for the potential dependence of θFe(II), of the polarization curves for cysteamine oxidation and the volcano correlation. n = 2, F = 96,485 C/mol, T = 298 K, $k_3 c_{OH^-} = 10$, $E_3^0 = 0$ V, $c = 0.005$, $k_2 = 3 \times 10^{-5}$, $E_2^0 = -0.3$ V, $E_{II/I}^0 = -0.9$ V, $E_{III/II}^0 = -0.4$ V.

where is the c is the weighed concentration of RSH, and applying the steady-state approximation to the concentration of the active intermediate $[Fe(II)N_4\text{-}RS]_{ads}$ in Eqs. (2) and (3), the following expression for the overall current density is obtained:

$$j = nFk_r(E,\Delta G_{ads})c_{OH^-}\theta[Fe(II)N_4\text{-}RS] = nFk_r(E,\Delta G_{ads})c_{OH^-}\frac{k_{ads}(E,\Delta G_{ads})c\theta[Fe(II)]}{k_{ads}(E,\Delta G_{ads})c\theta[Fe(II)] + k_{des}(E,\Delta G_{ads}) + k_r(E,\Delta G_{ads})c_{OH^-}} \quad (6)$$

where

$$k_{ads}(E,\Delta G_{ads}) = k_2\exp(\alpha_2 F(E - E_2^0)/RT)\exp(-\beta_2\Delta G_{ads}/RT) \quad (7)$$

$$k_{des}(E,\Delta G_{ads}) = k_2\exp(-(1-\alpha_2)F(E - E_2^0)/RT)\exp((1-\beta_2)\Delta G_{ads}/RT) \quad (8)$$

$$k_r(E,\Delta G_{ads}) = k_3\exp(\alpha_3 F(E - E_3^0)/RT)\exp((1-\beta_3)\Delta G_{ads}/RT) \quad (9)$$

θ[Fe(II)] represents the fraction of catalytic sites in the active Fe(II) state, ΔG_{ads} is the binding free energy of the RS· intermediate to the active state of the catalyst, k_{ads} and k_{des} are the rate constants of reaction (2), and k_r is the rate constant of reaction (3), and E_2^0 and E_3^0 are the corresponding standard equilibrium potentials. In Eqs. (6)–(8), we have assumed that all electron transfer reactions follow the Butler-Volmer rate law with transfer coefficients α_i, and that all reactions involving the adsorbed catalytic intermediate depend on its binding free energy following the Brønsted relation with Brønsted coefficients β_i (as originally suggested by Parsons [1]). In what follows, we will assume that all α_i and β_i are constant and equal to 0.5 and we will write them as α and β.

In the limit of weak adsorption, $\Delta G_{ads} \gg 0$ and $k_{des} \gg k_{ads}$, k_r, the current is given by

$$j = nFk_3\exp(-F(\alpha E_3^0 + E_2^0)/RT)\exp((1+\alpha)FE/RT)\exp(-\beta\Delta G_{ads}/RT) \quad (10a)$$

or, if $k_r \gg k_{ads}$, k_{des}:

$$j = nFk_2\exp(\alpha F(E - E_2^0)/RT)\exp(-\beta\Delta G_{ads}/RT) \quad (10b)$$

In the limit of strong adsorption, $\Delta G_{ads} \ll 0$ and $k_{ads} \gg k_{des} \gg k_r$, $\theta[Fe(II)N_4\text{ - }RS] = 1$ and the current is given by

$$j = nFk_3\exp(\alpha F(E - E_3^0)/RT)\exp((1-\beta)\Delta G_{ads}/RT) \quad (11)$$

Expressions (10a), (10b) and (11) are the limiting expressions for the two legs of the volcano, with the maximum of the volcano given approximately by the intersection of Eqs. (10a), (10b) and (11):

$$\Delta G_{ads} \approx F(E - E_2^0) \quad (12a)$$

$$\Delta G_{ads} \approx \alpha F(E_3^0 - E_2^0) + RT\ln\frac{k_2 c}{k_3 c_{OH^-}} \quad (12b)$$

Note that the Tafel slope is different on both sides of the volcano. In the limit of strong adsorption, the Tafel slope is predicted to be $\ln 10RT/\alpha F \approx 0.120$ V/dec. In the limit of weak adsorption, Eq. (10a) predicts a Tafel slope of $\ln 10RT/(1+\alpha)F \approx 0.040$ V/dec and Eq. (10b) a Tafel slope $\ln 10RT/\alpha F \approx 0.120$ V/dec.

If we assume a linear relation between the binding energy of the RS· intermediate and the Fe(II)/(I) redox transition, $\Delta G_{ads} = FE_{II/I}^0 + C$ (i.e., a more negative $E_{II/I}^0$ implying a stronger binding of the RS· intermediate), similarly to the linear correlation between M—O_2 binding energy and the M(III)/M(II) formal potential of the MN_4 catalyst observed for oxygen reduction [28], the linear correlations of the volcano plot can be expressed as a function of $E_{II/I}^0$ as:

$$j = nFk'\exp(-\beta FEI_{II/I}^0/RT) \quad (13)$$

$$j = nFk''\exp((1+\beta)FE_{II/I}^0/RT) \quad (14)$$

However, in the case of very negative redox potentials, the Fe(III)/(II) redox transition also comes into play, lowering the fraction of catalytically active sites θ[Fe(II)] with more positive potential, leading to the observed inhibition at higher potentials (see Figs. 4b, 5, and 6). Eqs. (1) and (6) together model the current-voltage curves and the volcano dependence of the cysteamine oxidation on Fe

Table 1
Formal potential of Fe(II)/(I) and Fe(III)/(II) processes of complexes deposited on OPG and on GC/MWCNT. Onset value of the polarization curve.

Complex	OPG/FeN4 complex				GC/MWCNT/FeN4 complex			
	$E^{o'}$Fe(II)/(I)	$E^{o'}$Fe(III)/(II)	Onset/V	Tafel slope/V	$E^{o'}$Fe(II)/(I)	$E^{o'}$Fe(III)/(II)	Onset/V	Tafel slope/V
FePc	− 0.624	− 0.177	− 0.405	0.064	− 0.684	− 0.171	− 0.490	0.059
16(Cl)FePc	− 0.307	− 0.055	− 0.421	0.110	− 0.272	− 0.061	− 0.542	0.098
FeTAPc	− 0.642	− 0.237	− 0.415	0.075	− 0.605	− 0.266	− 0.554	0.055
FeTNPc	− 0.610	− 0.255	− 0.463	0.089	− 0.660	− 0.256	− 0.576	0.061
FeTMeOP	− 1.388	− 0.639	− 0.339	0.122	− 1.365	− 0.655	− 0.355	0.154
FeTPyP	− 1.181	− 0.506	− 0.392	0.170	− 1.200	− 0.538	− 0.355	0.118

phthalocyanines. Fig. 10 shows some typical curves for representative values of the various model parameters, offering a semi-quantitative modeling of the experimental observations.

4. Conclusions

In this manuscript we demonstrate once more that the $M^{n+}/M^{(n-1)+}$ formal potentials of MN_4 macrocyclic molecular catalysts are very good reactivity descriptors for cysteamine electrooxidation and also for several electrochemical reactions. Most likely this parameter is a universal reactivity descriptor for redox mediators as in homogeneous redox catalysis [43]. One remarkable feature about this reactivity descriptor is that it can be easily determined experimentally under the same conditions of the kinetic measurements in contrast to other very good descriptors like binding energies of intermediates that need to be estimated from DFT calculations. Plots of activity as $(\log j)_E$ at constant E versus the $M^{n+}/M^{(n-1)+}$ redox potential give volcano correlations for both Fe(II)/(I) and Fe(III)/(II) formal potentials. It is possible to tune the $M^{n+}/M^{(n-1)+}$ redox potential of the MN4 catalyst by tailoring the electron-withdrawing character of the ligand of the macrocyclic complex to obtain the maximum activity. The catalytic activity of these FeN_4 species varies exponentially with the Fe (II)/(I) and Fe(III)/(II) redox potentials and plots of activity as $(\log j)_E$ versus E°Fe(II/I) and E°Fe(III/II) give volcano-shaped correlations for all electrodes, i.e. GC/FeN_4 and MWCNT/GC/FeN_4 configurations so a formal potential value exists for which the highest activity can be achieved. However, the maximum observed is not related to a value of $\Delta G_{ad}^{o} = 0$ as in classical activity volcano correlations but to a low surface concentration of Fe(II) active species for complexes having E° formal potentials close or more negative than the potential of the electrode at which activities are compared. It is interesting to note that for classical volcano correlation the hypothetical maximum activity is observed at ca. Fe(II)θ = 0.5, i.e. half of the active sites are occupied with adsorbed RS· molecules. In the present case the maximum should be close to a situation where θFe(II) = 0.5, i.e. where $\Gamma_{Fe(II)} = \Gamma_{Fe(III)}$as in the peak cyclic voltammogram and this would correspond to a hypothetical catalyst having $E^{\circ}_{(III/II)} = E^{\circ}_{max} = E$, where E is the electrode potential, i.e. − 0.3 V in this case. This value is very close the potential at which the maximum currents are observed in Fig. 8 and in the simulated volcano of Fig. 10.

Acknowledgements

The authors are grateful to Fondecyt Projects 1140199, Nucleo Milenio RC 120001, Fondecyt Postdoctoral Project 3150271, Conicyt Scholarships M.P.O. 21130168 and project AnilloACT-1412.

References

[1] R. Parsons, The rate of electrolytic hydrogen evolution and the heat of adsorption of hydrogen, Trans. Faraday Soc. 54 (1958) 1053–1063.
[2] R. Parsons, Volcano curves in electrochemistry in catalysis in electrochemistry, Fundamentals to Strategies for Fuel Cell Development, vol. 1, Wiley, 2011, pp. 1–15.
[3] A.B.P. Lever, Derivation of metallophthalocyanines Redox Potentials via Hammett parameter analysis, Inorg, Chim. Acta 203 (1993) 171–174.
[4] J.H. Zagal, S. Griveau, J.F. Silva, T. Nyokong, Metallophthalocyanine-based molecular materials as catalysts for electrochemical reactions, 254 (2010) 2755–2791 (Elsevier).
[5] Y.H. Tse, P. Janda, H. Lam, J. Zhang, W.J. Pietro, A.B.P. Lever, Monomeric and polymeric tetraaminophthalocyanatocobalt(II) modified electrodes: electrocatalytic reduction of oxyen, J. Porphyrins Phthalocyanines 1 (1997) 3–16.
[6] A.B.P. Lever, The phthalocyanines: moleules of enduring value, a two-dimensional analysis of redox potentials, J. Porphyrins Phthalocyanines 3 (1999) 488–499.
[7] S. Griveau, M. Gulppi, J. Pavez, J.H. Zagal, F. Bedioui, Cobalt phthalocyanine-based molecular materials for the electrocatalysis and electroanalysis of 2-mercaptoethanol, 2-mercaptoethanesulfonic acid, reduced glutathione and L-cysteine, Electroanalysis 15 (2003) 779–785.
[8] G. Cárdenas Jirón, J.H. Zagal, Donor–acceptor intermolecular hardness on charge transfer reactions of substituted cobalt phthalocyanines, J. Electroanal. Chem. 497 (2001) 55–60.
[9] R.O. Lezna, S. Juanto, J.H. Zagal, Spectroelectrochemical studies of tetrasulfonated metallophthalocyanines adsorbed on the basal plane of graphite in the presence of cysteine, J. Electroanal. Chem. 452 (1998) 221–228.
[10] M.J. Aguirre, M. Isaacs, F. Armijo, N. Bocchi, J.H. Zagal, Catalytic electrooxidation of 2-mercaptoethanol on perchlorinated iron phthalocyanine adsorbed on a graphite electrode, Electroanalysis 10 (1998) 571–575.
[11] C. Linares, D. Geraldo, M. Paez, J.H. Zagal, Non-linear correlations between formal potential and Hammett parameters of substituted iron phthalocyanines and catalytic activity for the electro-oxidation of hydrazine, J. Solid State Electrochem. 7 (2003) 626–631.
[12] J. Masa, K. Ozoemena, W. Schuhmann, J.H. Zagal, Oxygen reduction reaction using N-4-metallomacrocyclic catalysts: fundamentals on rational catalyst design, J. Porphyrins Phthalocyanines 16 (2012) 761–784.
[13] M.J. Aguirre, M. Isaacs, Armijo, Effect of the substituents on the ligand of iron phthalocyanines adsorbed on graphite electrodes on their activity for the electro-oxidation of 2-mercaptoethanol, Electroanalysis 14 (2002) 356–362.
[14] J.H. Zagal, S. Ureta-Zañartu, Electrocatalysis of hydrazine electrooxidation by phthalocyamines adsorbed on graphite, J. Electrochem. Soc. 129 (1982) 2242–2247.
[15] C. Caro, F. Bedioui, M.A. Páez, G.I. Cárdenas-Jiron, J.H. Zagal, Experimental and theoretical study of the activity of substituted metallophthalocyanines for nitrite electro-oxidation, J. Electrochem. Soc. 151 (2004) E32–E39.
[16] J.H. Zagal, C. Páez, Catalytic electrooxidation of 2-mercaptoethanol on a graphite electrode modified with metal-phthalocyanines, Electrochim. Acta 34 (1989) 243–247.
[17] R.K. Sen, J.H. Zagal, E. Yeager, The electrocatalysis of molecular oxygen reduction, Inorg. Chem. 16 (1977) 3379–3380.
[18] S. Habie, M. Bayo-Bangoura, K. Bayo, K. Servat, C. Morais, T.W. Napporn, K.B. Kokoh, Electrocatalytic activity of carbon-supported metallophthalocyanine catalysts towards oxygen reduction reaction in alkaline solution, J. Solid State Electrochem. 20 (2016) 931–942.
[19] C.S.J.N. O'Donoghue, M. Shumba, T. Nyokong, Electrode modification through click chemistry using Ni and Co alkynephthalocyanines for electrocatalytc detection of hydrazine, Electroanalysis 29 (2017) 1731–1740.
[20] S.R. Nxeke, P. Mashazi, T. Nyokong, Electrode modification using alkylnyl substituted Fe(II) phthalocyanine via electrografting and click chemistry for electrocatalysis, Electroanalysis 27 (2015) 2468–2478.
[21] E. Santos, W. Schmickler, Recent advances in theoretical aspects of electrocatalysis, Theory and Experiments in Electrocatalysis, vol. 50, Springer, 2010, pp. 25–88.
[22] M.T.M. Koper, Analysis of electrocatalytic reaction schemes: distinction between rate-determining and potential-determining steps, J. Solid State Electrochem. 17 (2013) 339–344.
[23] J.K. Norskov, J. Rossmeisl, A. Logadottir, L. Lindqvist, J.R. Kitchin, T. Bligaard, H. Jonsson, Origin of the overpotential for oxygen reduction at a fuel-cell cathode, J. Phys. Chem. 108 (2004) 17886–17892.
[24] M.T.M. Koper, Activity volcanoes for the electrocatalysis of homolytic and heterolytic hydrogen evolution, J. Solid State Electrochem. 20 (2016) 895–899.
[25] F. Calle, J.I. Martínez, J.M. García, E. Abad, M.T.M. Koper, Oxygen reduction and evolution at single-metal active sites: comparison between functionalized graphitic materials and protoporphyrins, Surf. Sci. 607 (2013) 47–53.
[26] M.T.M. Koper, Thermodynamic theory of multi-electron transfer reactions: implications for electrocatalysis, J. Electroanal. Chem. 660 (2011) 254–260.
[27] M.T.M. Koper, Combining experiment and theory for understanding electrocatalysis, J. Electroanal. Chem. 574 (2005) 375–386.
[28] J.H. Zagal, M.T.M. Koper, Reactivity descriptors for the activity of MN4 molecular catalysts for the oxygen reduction reaction, Angew. Chem. Int. Ed. 55 (2016) 14510–14521.
[29] D.A. Scherson, Electrocatalysis at microelectrodes: geometrical considerations, J. Phys. Chem. C 114 (2010) 13650–13656.
[30] J.E. Biaglow, R.W. Issels, L.E. Gerweck, M.E. Varnes, B. Jacobson, J.B. Mitchell, A. Russo, Factors influencing the oxidation of cysteamine and other thiols: implications for hyperthermic sensitization and radiation protection, Radiat. Res. Soc. 100 (1984) 298–312.
[31] M. Keyvanfard, S. Sami, H. Karimi-Maleh, K. Alizad, Electrocatalytic determination of cysteamine using multiwall carbon nanotube paste electrode in the presence of 3,4-dihydroxycinnamic acid as a homogeneous mediator, J. Braz. Chem. Soc. 24 (2013) 32–39.
[32] M. Keyvanfard, A.A. Ensafi, H. Karimi-Maleh, A new strategy for simultaneous determination of cysteamine in the presence of high concentration of tryptophan using vinylferrocene-modified multiwall carbon nanotubes paste electrode, J. Solid State Electrochem. 16 (2012) 2949–2955.
[33] A. Michota, A. Kudelski, J. Bukowska, Chemisorption of cysteamine on silver studied by surface-enhanced Raman scattering, J. Am. Chem. Soc. 16 (2000) 10236–10242.
[34] V. Arabali, H. Karimi-Maleh, Electrochemical determination of cysteamine in the presence of guanine and adenine using a carbon paste electrode modified with N-(4-hydroxyphenyl)-3,5-dinitrobenzamide and magnesium oxide nanoparticles, J. Anal. Methods 8 (2016) 5604–5610.
[35] A.A. Ensafi, H. Karimi-Maleh, A. Voltammetric Sensor, Based on modified multiwall carbon nanotubes for cysteamine determination in the presence of tryptophan using *p*-aminophenol as a mediator, Electroanalysis 22 (2010) 2558–2568.
[36] V.V. Apyari, S.G. Dmitrienko, V.V. Arkhipova, Y.A. Zolotov, Determination of cysteamine using label-free gold nanoparticles, J, Anal. Methods 4 (2012) 3193–3199.
[37] I.S. El-Hallag, A.O. Al-Youbi, A.Y. Obaid, E.H. El-Mossalamy, S.A. El-Daly, A.M. Asiri, Electro chemical investigation of cysteamine at carbon fiber microdisdk electrode, J. Chil. Chem. Soc. 56 (2011) 837–841.
[38] F. Bedioui, S. Griveau, T. Nyokong, A.J. Appleby, C.A. Caro, G. Ochoa, J.H. Zagal,

Tuning the redox properties of metalloporphyrin and metallophthalocyanine based molecular electrodes for the highest electrocatalytic activity for the oxidation of thiols, Phys. Chem. Chem. Phys. 9 (2007) 3383–3396.
[39] C.A. Gutierrez, J.F. Silva, F.J. Recio, S. Griveau, F. Bedioui, C.A. Caro, J.H. Zagal, In search of the best iron N4-macrocyclic catalysts adsorbed on graphite electrodes and on multi-walled carbon nanotubes for the oxidation of L-cysteine by adjusting the Fe(II)/(I) formal potential of the complex, Electrocatalysis 5 (2014) 426–437.
[40] B.S. Paunkovic, C.E. Banks, R.G. Compton, An overview of the electrochemical reduction of oxygen at carbon-based modified electrodes, J. Iran. Chem. Soc. 2 (2005) 1–13.
[41] A. Alsudairi, J. Li, N. Ramaswamy, S. Mukerjee, K.M. Abraham, Q. Jia, Resolving the iron phthalocyanine redox transitions for ORR catalysis in aqueous media, J. Phys. Chem. Lett. 8 (2017) 2881–2886.
[42] M. Pérez-Mendoza, C. Schuhmacher, F. Suarez-Garcia, M.C. Almazan-Almazan, M. Domingo-Garcia, F.J. Lopez-Garzon, N.A. Seaton, Analysis of the microporous texture of a glassy carbon by adsorption measurements and Monte Carlo simulation. Evolutionwith chemical and physical activation, Carbon 44 (2006) 638–645.
[43] S.B. Han, D.-H. Kwak, H.S. Park, I.-A. Choi, J.-Y. Park, K.-B. Ma, J.-E. Won, D.-H. Kim, S.-J. Kim, M.-C. Kim, K.-W. Park, Chemically regenerative redox-fuel cells using iron redox couples as a liquid catalyst with cocatalysts, ACS Catal. 6 (2016) 5302–5306.